Acta Oceanol. Sin., 2019, Vol. 38, No. 4, P. 80–89
https://doi.org/10.1007/s13131-019-1415-5
http://www.hyxb.org.cn
E-mail: hyxbe@263.net

Characteristics and temporal variations of near-bottom currents near the Dongsha Island in the northern South China Sea

Dawei Li[1, 2], Zexun Wei[1, 2]*, Yonggang Wang[1, 2], Shujiang Li[1, 2], Tengfei Xu[1, 2], Guanlin Wang[1, 2], Fei Teng[1, 2]

[1] Key Laboratory of Marine Science and Numerical Modeling, First Institute of Oceanography, Ministry of Natural Resources, Qingdao 266061, China

[2] Laboratory for Regional Oceanography and Numerical Modeling, Pilot National Laboratory for Marine Science and Technology (Qingdao), Qingdao 266237, China

Received 20 June 2018; accepted 11 October 2018

Abstract

Near-bottom currents play important roles in the formation and dynamics of deep-water sedimentary systems. This study examined the characteristics and temporal variations of near-bottom currents, especially the tidal components, based on two campaigns (2014 and 2016) of *in situ* observations conducted southeast of the Dongsha Island in the South China Sea. Results demonstrated near-bottom currents are dominated by tidal currents, the variance of which could account for ~70% of the total current variance. Diurnal tidal currents were found stronger than semidiurnal currents for both barotropic and baroclinic components. The diurnal tidal currents were found polarized with predominantly clockwise-rotating constituents, whereas the clockwise and counterclockwise constituents were found comparable for semidiurnal tidal currents. It was established that diurnal tidal currents could induce strong current shear. Baroclinic tidal currents showed pronounced seasonal variation with large magnitude in winter and summer and weak magnitude in spring and autumn in 2014. The coherent components accounted for ~65% and ~50% of the diurnal and semidiurnal tidal current variances, respectively. The proportions of the coherent and incoherent components changed little in different seasons. In addition to tidal currents, it was determined that the passing of mesoscale eddies could induce strong near-bottom currents that have considerable influence on the deep circulation.

Key words: tidal currents, South China Sea, near-bottom currents, mesoscale eddies

Citation: Li Dawei, Wei Zexun, Wang Yonggang, Li Shujiang, Xu Tengfei, Wang Guanlin, Teng Fei. 2019. Characteristics and temporal variations of near-bottom currents near the Dongsha Island in the northern South China Sea. Acta Oceanologica Sinica, 38(4): 80–89, doi: 10.1007/s13131-019-1415-5

1 Introduction

The South China Sea (SCS), with bathymetry that varies from <100 m on the continental shelf to >4 000 m in the deep basin, is the largest semienclosed marginal sea in the West Pacific Ocean. Mainly driven by the East Asian Monsoon, the upper circulation in the SCS shows obvious seasonal characteristics with a cyclonic pattern in winter and an anticyclonic pattern in summer (Hu et al., 2000). Previous studies have made considerable progress in elucidating the characteristics and seasonal variations of the upper-layer circulation on the continental slope of the northern South China Sea (NSCS) (Shu et al., 2018). It is commonly recognized that the SCS deep circulation at depths >2 000 m is a basin-scale cyclonic circulation (Li and Qu, 2006; Wang et al., 2011). Using the Hybrid Coordinate Ocean Model, Lan et al. (2013) provided a description of the SCS deep circulation, and they found that the basin-scale cyclonic deep circulation was controlled by the Luzon Strait overflow. Lan et al. (2015) revealed that the deep circulation shows obvious seasonal variation with a basin-scale cyclonic gyre that is strong in summer and weak in winter. However, because of the complex bathymetry and lack of observations, the deep-water properties and the dynamics of the deep circulation in the SCS remain poorly understood.

Previous studies have demonstrated that the deep circulation, especially the near-bottom currents, have important effects on deep-water sedimentary systems, including the sediment formation and dynamics (Lei et al., 2007; Zheng and Yan, 2012; Chen et al., 2016). The interactions among multiscale dynamic processes and complex bathymetry are known to play important roles in the deep circulation, sediment transport, and abyssal carbon cycle of the NSCS (Su, 2004). Moreover, the NSCS has been found to have strong internal tides in comparison with other seas (Duda et al., 2004; Guo et al., 2012; Lee et al., 2012). After generation in the Luzon Strait, internal tides propagate westward into the deep basin of the NSCS and then travel onto the continental shelf as baroclinic waves (Alford et al., 2015; Beardsley et al., 2004). During propagation, their energy dissipates because of mixing pro-

Foundation item: The National Key Research and Development Program of China under contract No. 2017YFC1404201; the National Natural Science Foundation of China under contract Nos 41706035 and 41876029; the NSFC-Shandong Joint Fund for Marine Science Research Centers under contract No. U1606405; the Laboratory for Regional Oceanography and Numerical Modeling, Qingdao National Laboratory for Marine Science and Technology under contract No. 2017A01; the China Postdoctoral Science Foundation under contract No. 2017M622111.

*Corresponding author, E-mail: weizx@fio.org.cn

cesses, accompanied by the generation of internal solitary waves on the NSCS shelf (Zhao et al., 2004; Zheng et al., 2007). In particular, the region east of Dongsha Island in the SCS is an area of transition from the deep basin to the continental slope/shelf. The bathymetry in this region changes dramatically from depths of >3 000 m to hundreds of meters, which might constrain bottom flow paths and could trigger strong internal tides (Klymak et al., 2011; Lien et al., 2005). Using results from numerical models, Alford et al. (2015) examined the importance of the region between 117.89°E and 117.25°E on internal tide flux and energy transport, and they found the continental slope east of Dongsha Island was a region "critical" for internal tide conversion.

With respect to near-bottom currents, our understanding remains poor because of the lack of high-resolution *in situ* observations over wide temporal ranges. Therefore, the characteristics of tidal currents should be further examined. Given this consideration, we conducted two campaigns of observations southeast of Dongsha Island (20.3°N, 117.6°E), to examine the characteristics and temporal variations of near-bottom currents. The remainder of this paper is organized as follows. The observation system used in the study is described in Section 2. An overview of the near-bottom currents is presented in Section 3. The tidal currents are analyzed in detail in Section 4. In Section 5, we discuss the characteristics of tidal currents and the influence of an anticyclonic eddy on the near-bottom currents. Finally, Section 6 presents a brief summary.

2 Data

The site selected for the observations is located in the NSCS, as depicted in Fig. 1. The water depth at this location is 2 224 m. Two observational deployments were conducted, the first from September 19, 2014 to September 16, 2015 and the second from September 24, 2016 to June 25, 2017. During the first deployment, two AANDERAA SeaGuard Single Point Current Meters (CMs), placed 24 and 81 m above the ocean bottom (hereafter, D1U-CM and D1D-CM, respectively), were used to measure the deep-ocean currents at 1-h intervals. An SBE 37 CTD placed 80 m above the ocean bottom was used to measure the pressure, temperature, and salinity at 5-min intervals. During the second deployment, a CM was placed 30 m above the ocean bottom (hereafter, D2-CM) and an SBE 37 CTD was mounted 1 m beneath this CM. The currents observed by the CMs were rotated counterclockwise (CCW) by 30° for transformation into along- and cross-isobath components. The configurations of the observation system are given in Table 1.

3 Basic characteristics

Time series of the original along- and cross-isobath velocities observed by D1U-CM, D1D-CM, and D2-CM are shown in Fig. 2. The velocities range from –20 to 20 cm/s with mean magnitude of 6.42 cm/s for the along-isobath component and 5.66 cm/s for the cross-isobath component. To obtain the subtidal currents, a 3-d Butterworth low-pass filter was applied to exclude the inertial (~34 h at the observation site) and tidal components, and the derived results are shown by the black lines in Fig. 2. It can be seen that the along-isobath subtidal component is stronger than the cross-isobath component. The along-isobath subtidal component has a root mean square (RMS) of 1.82 cm/s, which is more than twice that of the cross-isobath component (0.78 cm/s). High-frequency fluctuations, which are mainly because of the tidal currents, are evident in both the along- and the cross-isobath original velocity time series. We applied a high-pass filter with a cutoff period of 48 h to the original time series and found that the variances ($V_a = u^2 + v^2$, where u and v are the along- and cross-isobath currents, respectively) of the high-frequency components accounted for ~67% and ~73% of the total current variance for the along- and cross-isobath currents, respectively. The mean magnitude is 4.01 cm/s for the along-isobath high-pass component and 3.86 cm/s for the cross-isobath high-pass component.

To further examine the temporal and frequency distributions of the along- and cross-isobath velocities at the observation site, the wavelet power spectrum method (Torrence and Compo, 1998) was resorted. As shown in Fig. 3, diurnal tidal currents dominate both the along- and the cross-isobath components. The wavelet power spectra also demonstrate signals of semidi-

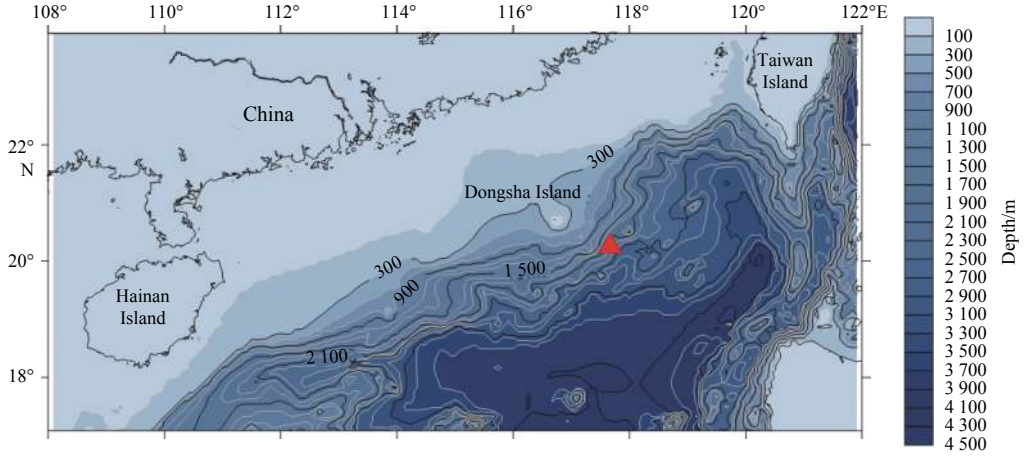

Fig. 1. Bathymetry of the NSCS. Color shading denotes depth and the red triangle identifies the location of the observation site.

Table 1. Observation system configurations

Mooring	Location	Depth/m	Recording period (day/month/year)	Instrument depth/m
D1	20.3°N, 117.6°E	2 224	19/09/2014–16/09/2015	CM: 2 200 and 2 143, CTD: 2 144
D2	20.3°N, 117.6°E	2 224	24/09/2016–25/06/2017	CM: 2 194, CTD: 2 195

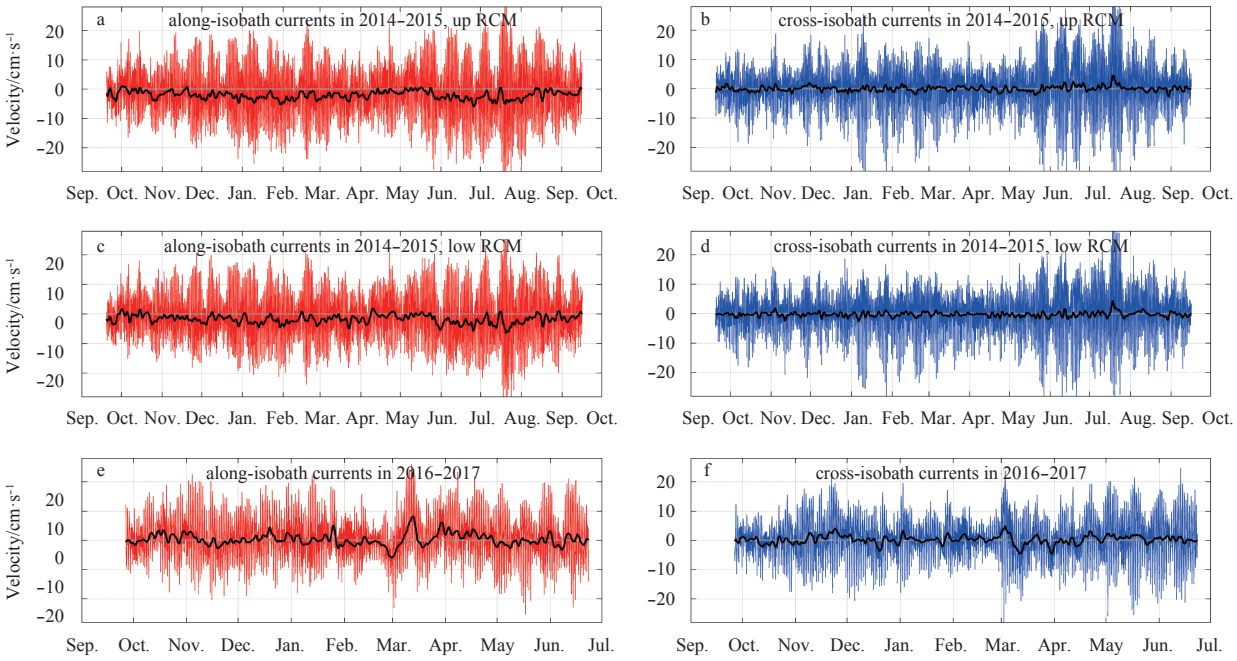

Fig. 2. Time series of velocities observed by D1U-CM (a, b), D1D-CM (c, d), and D2-CM (e, f). Left-hand panels show along-isobath components and right-hand panels cross-isobath components. Thick black lines show the results obtained after applying a 3-d low-pass filter to the original data.

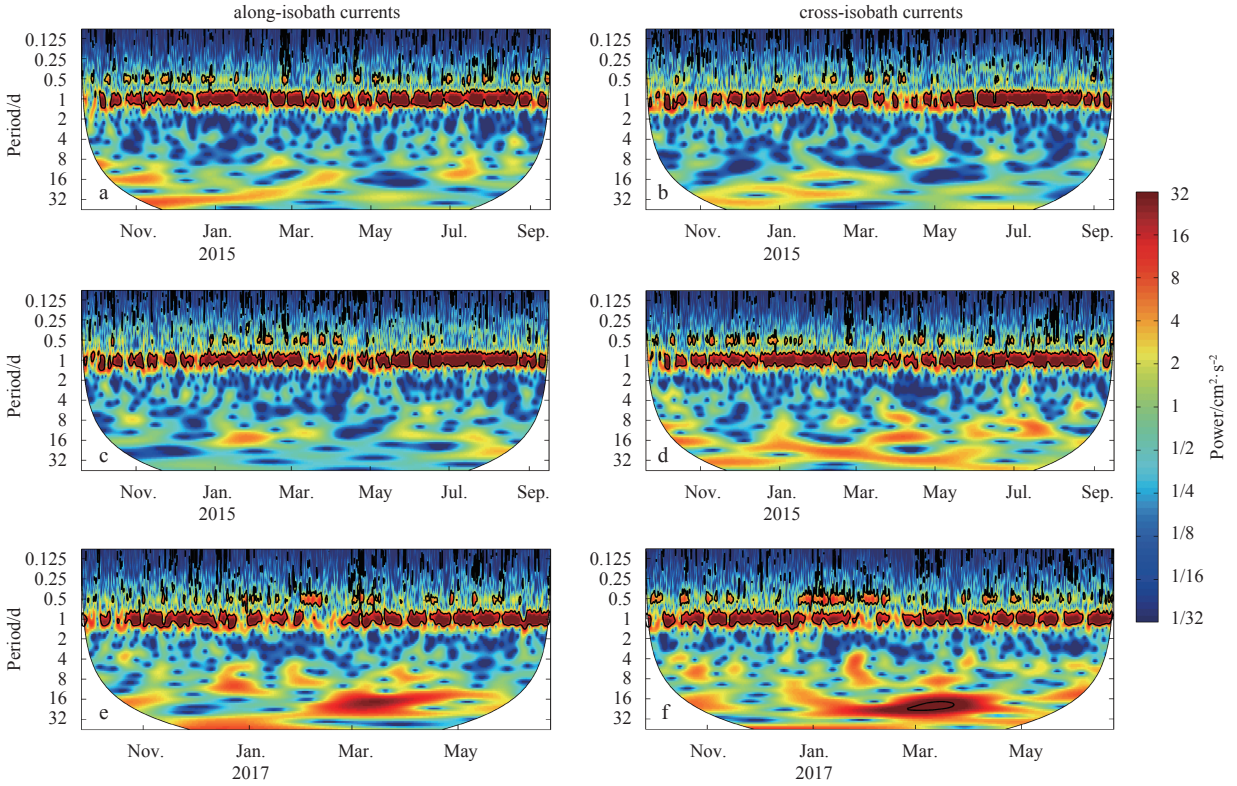

Fig. 3. Continuous wavelet power spectra of along- and cross-isobath currents of D1U-CM (a, b), D1D-CM (c, d), and D2-CM (e, f). Thick black lines denote the 95% confidence level, and thin black lines the region affected by the edges of data.

urnal currents with magnitudes much weaker than the diurnal tidal currents. As for the second observational deployment (Figs 3e and f), strong signals with period of ~25 d are evident during March and April 2017, associated with the passing of an anticyclonic mesoscale eddy shed from the Kuroshio Loop.

The rotary spectra were used to interpret the inherent rotational characteristics of the near-bottom currents in different frequency bands. Rotary spectra decompose a complex velocity

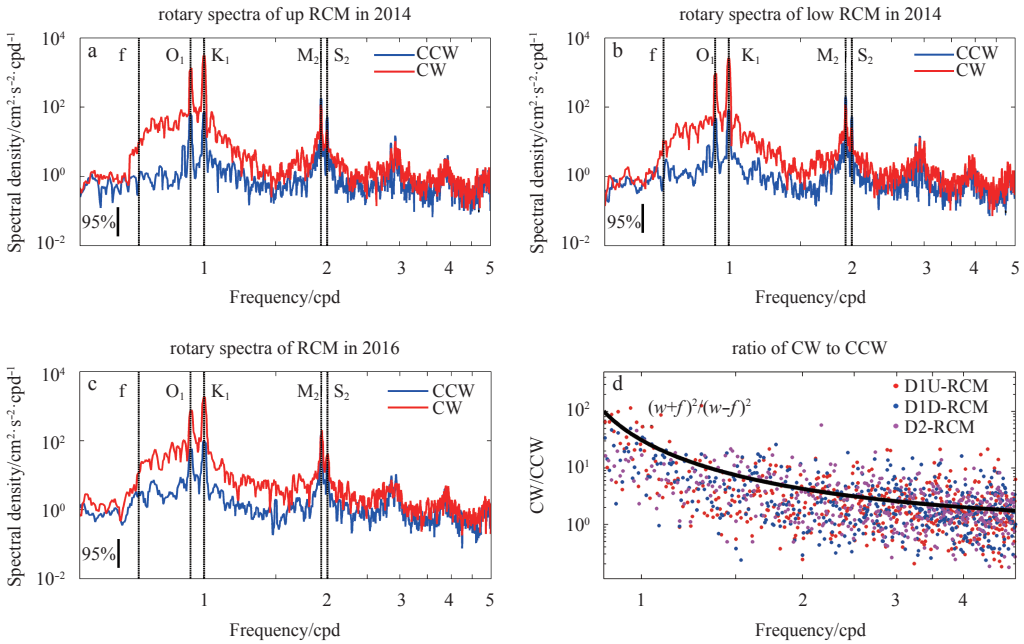

Fig. 4. Rotary spectra of currents obtained by D1U-CM (a), D1D-CM (b), and D2-CM (c); and the observed and theoretical CW/CCW ratios (d). Red (blue) lines represent the CW (CCW) rotating components. Vertical lines denote the local inertial frequency and major diurnal and semidiurnal tidal frequencies.

(u+iv) into clockwise (CW) and CCW rotating components (Gonella, 1972). The results of the rotary spectra (Fig. 4) show multiple peaks at different frequencies, e.g., the inertial frequency (f), diurnal tidal frequencies O_1 and K_1, and semidiurnal tidal frequencies M_2 and S_2. There are also energy peaks at the compound (8 h), second harmonic (6 h), and higher harmonics, indicating strong nonlinearity of the internal tides. The CW components are larger than the CCW components in the rotary spectra, which is consistent with the internal wave theory for the Northern Hemisphere. The amplitude ratio of the CW and CCW components is ~10 for the diurnal band and the ratio decreases with increasing frequency. At the semidiurnal frequency band, the CW and CCW components are comparable. Based on the free internal wave theory, the theoretical ratio of CW and CCW components follows the line of $(\omega+f)^2/(\omega-f)^2$, where f is the local inertial frequency and ω is the internal wave frequency (Garrett and Kunze, 2007). We compared the observed CW/CCW ratio to the theoretical ratio (Fig. 4d) and found that the observed ratio is close to the theoretical ratio, although the observed ratio is slightly smaller than the theoretical ratio for the diurnal frequency band.

As the vertical shear of the horizontal velocity is associated with the stability of the water column and ocean mixing, we used the shear spectrum to analyze the vertical shear in the near-bottom layer. The vertical shear (s_h) of the horizontal current between D1U-CM and D1D-CM is defined as

$$s_h^2 = \left(\frac{\partial U}{\partial z}\right)^2 + \left(\frac{\partial V}{\partial z}\right)^2. \quad (1)$$

As shown in Fig. 5, the vertical shear exhibits pronounced peaks near the diurnal frequencies (O_1 and K_1), which means the diurnal tidal currents dominate the vertical current shear and contribute most to deep-ocean mixing.

4 Tidal currents

As shown in the above section, the near-bottom currents at the observation site are dominated by tidal currents. In this section, we analyze the characteristics and temporal variations of the tidal currents in detail.

4.1 *Barotropic constituent*

Barotropic tides can cause variation of sea surface elevation that could influence the depth of moored instruments. In our observational campaigns, an SBE37 CTD was deployed at a depth of >2 000 m. At this depth, vertical motion of the moored instrument is weak and any depth fluctuation could be attributed mainly to variation of the sea surface elevation caused by barotropic tides. In this paper, we define depth fluctuation as the original depth time series recorded by the SBE37 minus the mean depth over the entire observational period. The time series of depth fluctuations are shown in Fig. 6. Tidal motions with a spring–neap cycle of ~14 d are clearly visible. At spring tides, the amplitude of depth fluctuation of the SBE37 is >0.5 m (Figs 6a and c). The power spectra of depth fluctuations show that prominent peaks occur in the diurnal and semidiurnal frequency bands (Figs 6b and d). The diurnal tides are stronger than the semidiurnal tides. The primary tidal constituents consist of the diurnal frequencies O_1 and K_1, and the semidiurnal frequencies of M_2 and S_2. There also are energy peaks at higher harmonics, reflecting the strong nonlinearity of barotropic tides.

4.2 *Baroclinic tidal ellipse*

Baroclinic tidal currents are usually estimated by vertically averaging full-depth measurements. However, in our study, we observed currents at only two fixed depth near the seafloor. Therefore, we used OSU tidal prediction software (OTPS) (Egbert and Erofeeva, 2002; http://volkov.oce.orst.edu/tides/TPXO7.2.html) to obtain the barotropic currents. The baroclinic tidal currents were obtained by subtracting the OTPS-predicted barotropic currents from the observed original data. Then, to

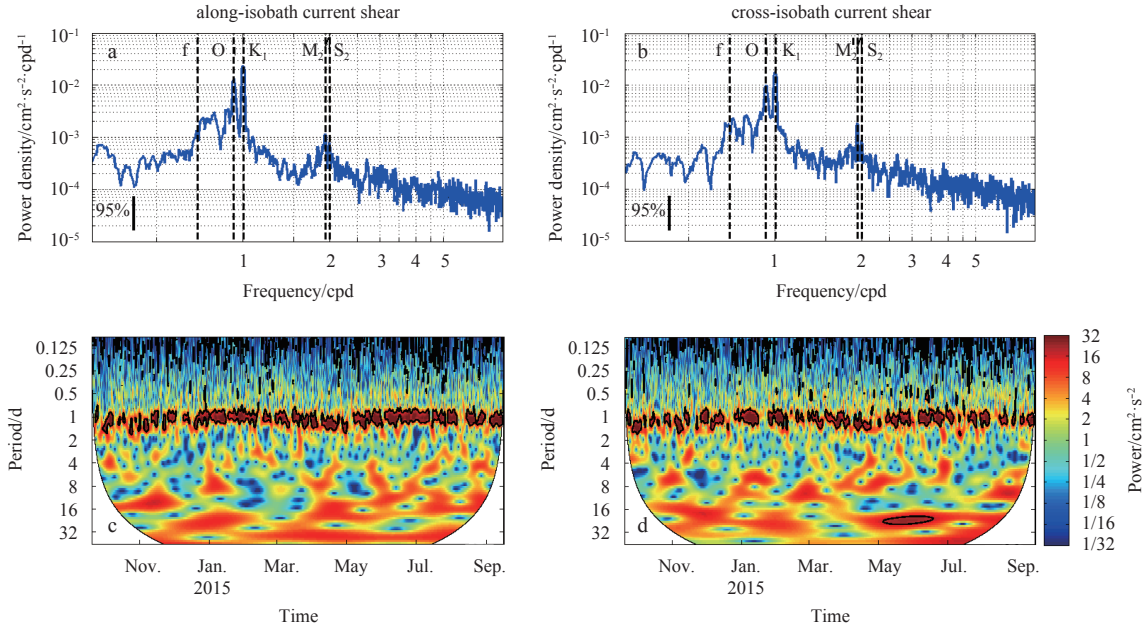

Fig. 5. Along-isobath shear (a) and the cross-isobath shear (b) spectrums between D1U-CM and D1D-CM; and continuous wavelet power spectrums of along-isobath shear (c) and cross-isobath shear (d) between D1U-CM and D1D-CM.

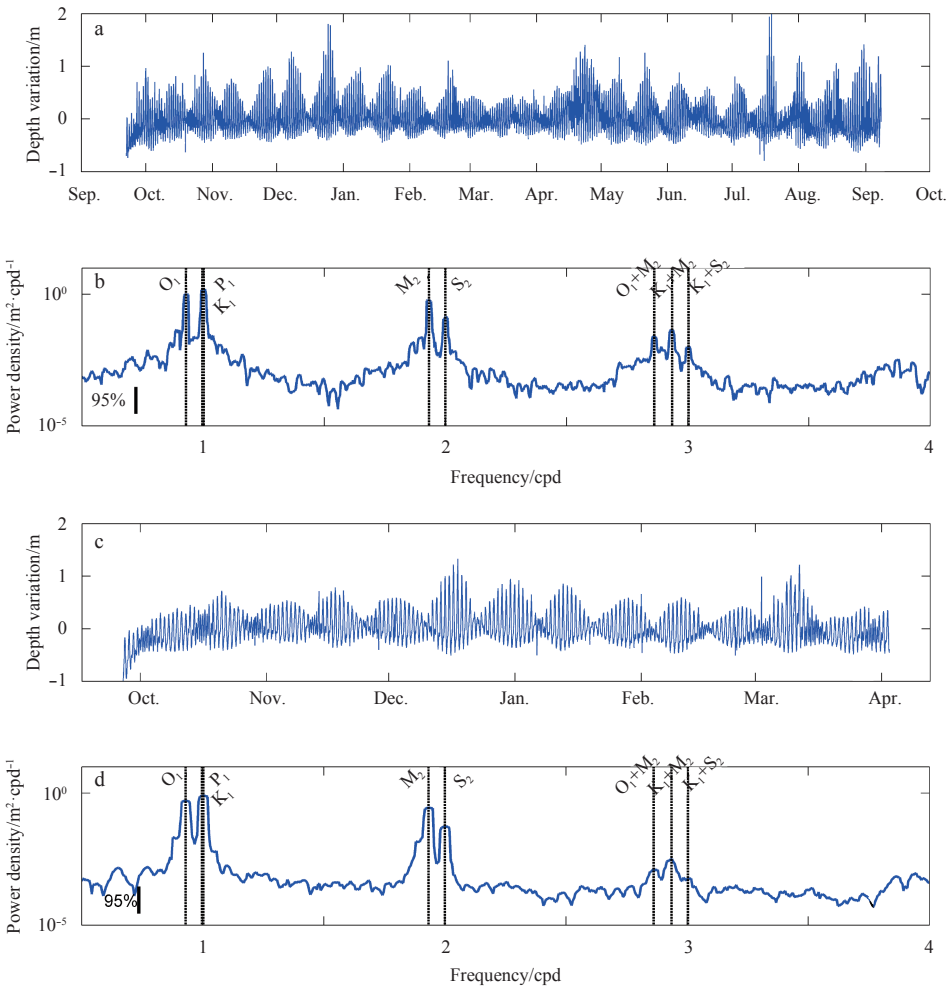

Fig. 6. Time series of depth fluctuation obtained from SBE 37 CTD data during the first (a) and the second (c) observational campaigns, and power density spectra of depth fluctuation during the first (b) and the second (d) observational campaigns. Vertical lines indicate major diurnal and semidiurnal tidal frequencies.

compare the characteristics of the primary baroclinic tidal constituents, harmonic analysis was performed on the baroclinic currents using the Matlab program T_Tide (Pawlowicz et al., 2002). The characteristics of the baroclinic tides during the entire observational period can be illustrated based on the results of the harmonic analysis.

Tidal ellipses of the major diurnal and semidiurnal baroclinic constituents are shown in Fig. 7. The ellipse properties of the major diurnal and semidiurnal baroclinic tidal constituents are given in Table 2. The semimajor axes of the baroclinic constituents O_1, K_1, M_2 and S_2 are 4.49, 6.49, 2.62 and 1.09 cm/s, respectively. All of the four tidal constituents turn CW. The ratio $(H_{O_1} + H_{K_1})/(H_{M_2} + H_{S_2})$ is 2.96, which means the baroclinic tides are mixed with diurnal constituents dominant.

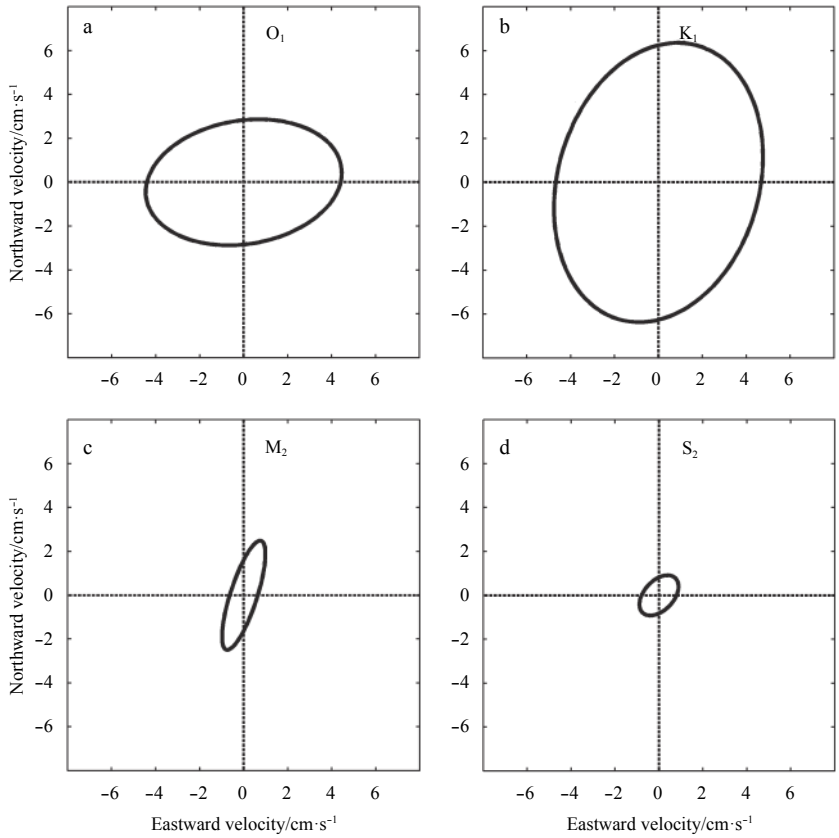

Fig. 7. Tidal ellipses of the major diurnal and semidiurnal baroclinic constituents.

Table 2. Ellipse properties of the major diurnal and semidiurnal baroclinic tidal constituents

Constitutes	Semi-major axis/cm·s^{-1}	Semi-minor axis/cm·s^{-1}	Inclination/(°)	Phase/(°)
O_1	4.494	–2.813	9.27	22.76
K_1	6.488	–4.588	74.03	62.73
M_2	2.617	0.615	72.30	43.46
S_2	1.089	0.677	46.89	72.69

4.3 *Temporal variations*

To further study the temporal variations of the internal tides, a band-pass filter was applied to the original data, and the diurnal (0.85–1.15 cpd) and semidiurnal (1.85–2.15 cpd) baroclinic tidal currents during the two observational campaigns are shown in Figs 8 and 9, respectively. To aid understanding of the seasonal variability of the baroclinic tides at the observation site, we also display time series of the barotropic diurnal and semidiurnal tidal components obtained from the OTPS (black lines in Figs 8 and 9). The diurnal tidal currents demonstrate obvious seasonal variation. In 2014, the diurnal tidal currents are strong in summer and winter and weak in spring and autumn for both the along- and cross-isobath components. The maximum amplitude in summer is up to 20 cm/s. However, the temporal variation in 2016 shows a different pattern with weak amplitude in winter.

As for the semidiurnal components, the amplitude is smaller compared with the diurnal baroclinic currents, i.e., the maximum value is no more than 10 cm/s. In comparison with the diurnal baroclinic tides, the seasonal variation of the semidiurnal baroclinic tides is less apparent and the pattern is more complex. The along-isobath component has greater amplitude in winter, whereas the cross-isobath component has smaller amplitude in winter.

4.4 *Coherent and incoherent components*

Previous studies have shown that the coherent and incoherent features of internal tides could change during propagation because of modulation by the background conditions and stratification (Lee et al., 2012; Xu et al., 2013; Cao et al., 2017). Standard tidal harmonic analysis was applied to the full record to explore the degree of coherence (phase locked) with astronomical forcing at the observation site. We also calculated the variances of the coherent and incoherent components for the diurnal and semidiurnal tidal currents and the time series are shown in Fig. 10. The coherent variances account for about ~65% and ~50% of the

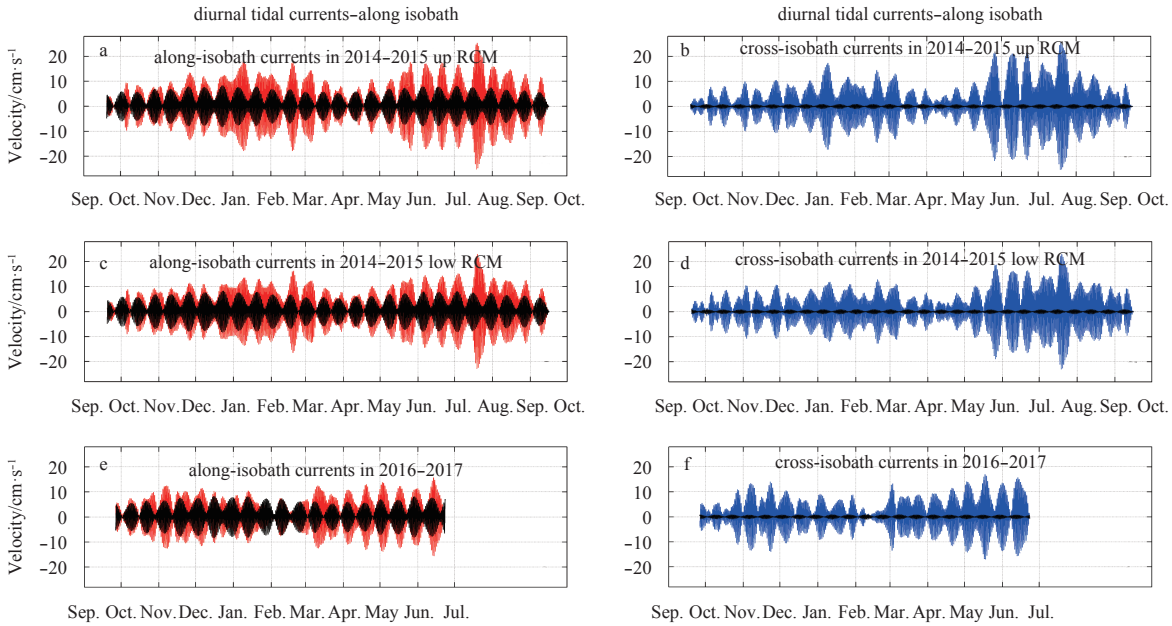

Fig. 8. Time series of along- and cross-isobath diurnal baroclinic currents observed by D1U-CM (a, b), D1D-CM (c, d), and D2-CM (e, f). Black lines indicate barotropic tides obtained from the OTPS.

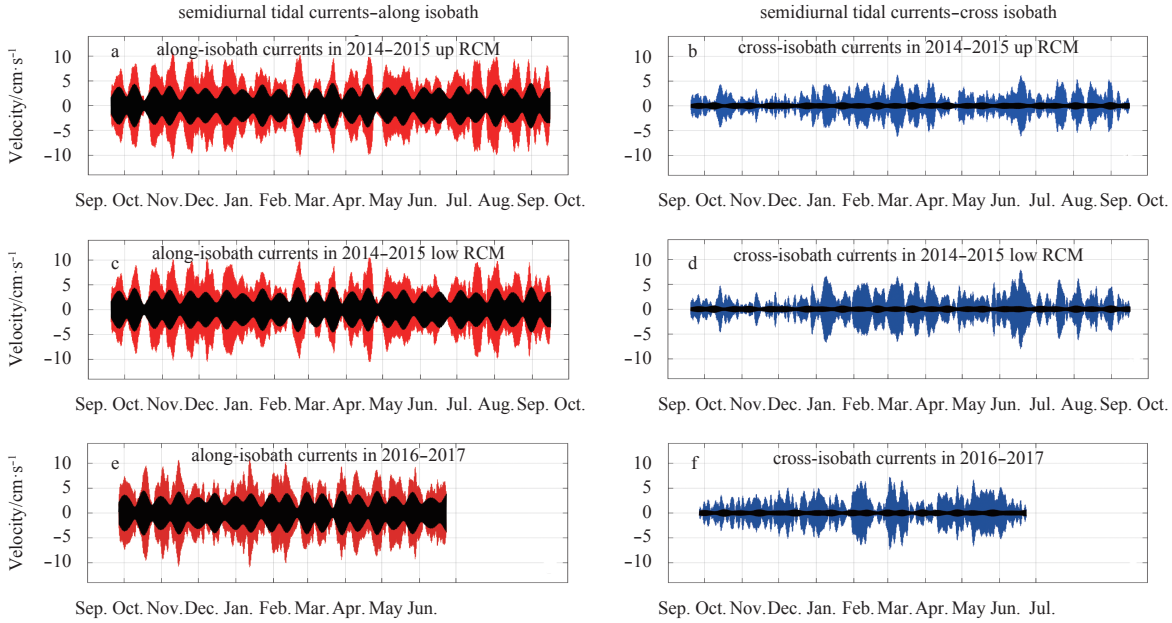

Fig. 9. Time series of along- and cross-isobath semidiurnal baroclinic currents observed by D1U-CM (a, b), D1D-CM (c, d), and D2-CM (e, f). Black lines indicate barotropic tides obtained from the OTPS.

variances of the diurnal and semidiurnal baroclinic tides, respectively. The proportions of the coherent and incoherent components do not change significantly in different seasons (Fig. 11).

5 Discussion

Previous studies have documented that the continental slope and shelf near Dongsha Island is a region critical for barotropic-to-baroclinic conversion (Alford et al., 2015; Klymak et al., 2011). Klymak et al. (2011) found that the continental slope near Dongsha Island is supercritical with respect to the diurnal tide and subcritical with respect to the semidiurnal tide. After generation in Luzon Strait, the diurnal tide reaches the continental slope and one third is reflected back into the basin, whereas the observed reflection is very weak for semidiurnal tides. Thus, the model structure of internal tides could also be changed substantially, accompanied by the generation of internal solitary waves on the continental slope and shelf of the NSCS (Zhao et al., 2004; Zheng et al., 2007). According to the results of numerical simulation by Alford et al. (2015), integrated semidiurnal tidal fluxes and nonlinear internal wave fluxes increase significantly and diurnal fluxes decrease on the continental slope near Dongsha Island. Continuous observations are needed to explore the detailed barotropic-to-baroclinic conversion processes in this area.

Baroclinic tides in the northern SCS are associated with baro-

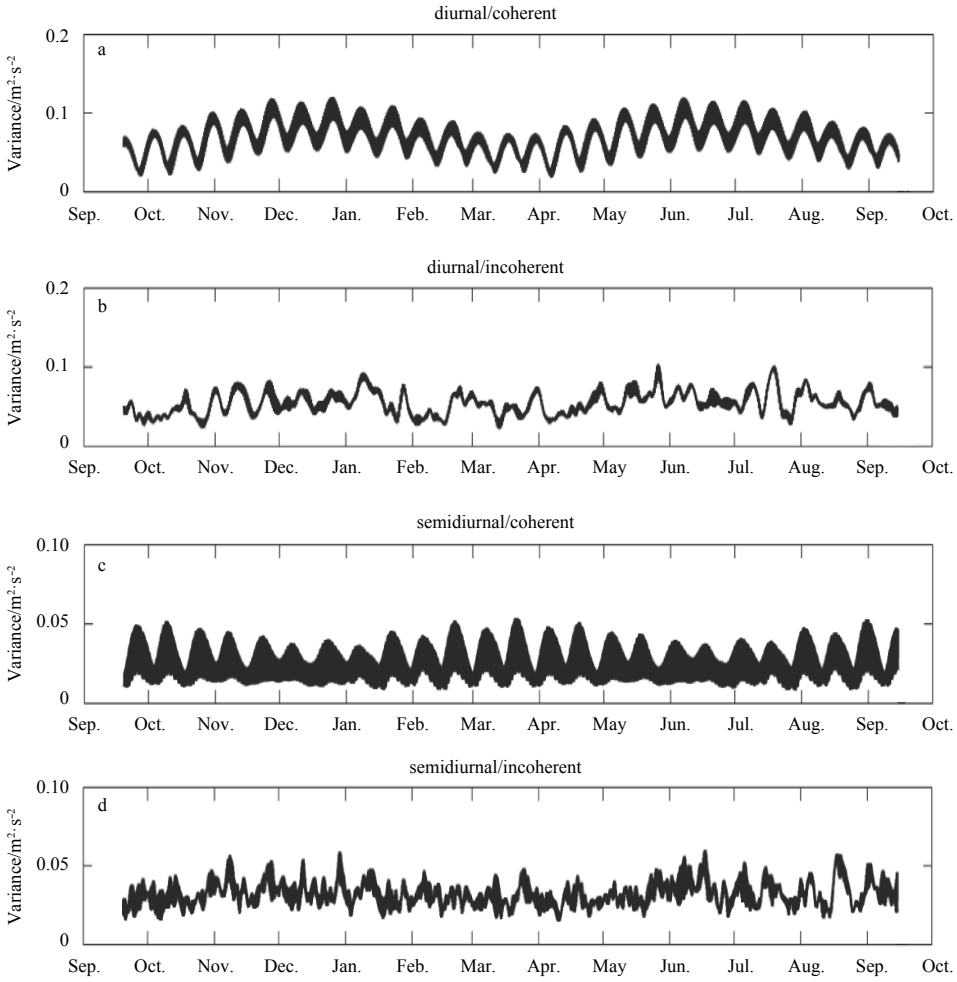

Fig. 10. Coherent and incoherent diurnal tidal currents (a, b) and semidiurnal tidal currents (c, d), respectively.

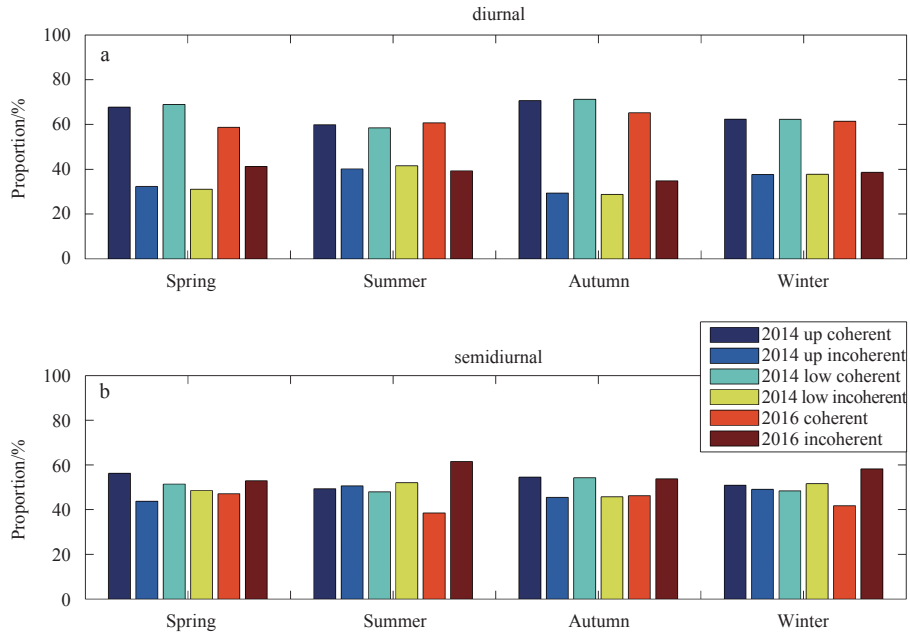

Fig. 11. Proportions of coherent and incoherent components in different seasons for diurnal currents (a) and semidiurnal currents (b).

tropic tidal forcing and stratification. Previous studies have found that baroclinic tides across the NSCS demonstrate obvious seasonal variability, although the patterns are different at different observation sites. For example, Guo et al. (2012) found that both diurnal and semidiurnal baroclinic tides on the continental shelf were strong in both spring and autumn but weak in winter. Ma et al. (2013) found that diurnal baroclinic currents on the continental slope were weakest in spring and strongest in summer, although less seasonal variability was observed on the continental shelf. Xu et al. (2013) found that diurnal baroclinic tides had greatest amplitude in summer and smallest amplitude in winter, whereas no obvious seasonal variations were found for semidiurnal baroclinic tides. Based on observations in the NSCS, Cao et al. (2017) reported that diurnal baroclinic tides were strongest in winter and summer but weakest in spring and autumn.

In our study, in combination with the temporal variations of the barotropic tidal currents derived from the OTPS (Fig. 8a), it can be concluded that the seasonal variability of the along-isobath baroclinic tides is determined mainly by the barotropic tides. As for the cross-isobath baroclinic tidal currents, their magnitudes are much larger than the barotropic tidal currents and their direction of flow is perpendicular to the slope, which suggests the cross-isobath baroclinic tidal currents at the observation site might be generated locally. Further observations and additional background information are needed to analyze the difference in the behavior of baroclinic tides in different years.

Variation of the background conditions and stratification could modulate the coherent and incoherent features of an internal tide during its propagation (Lee et al., 2012; Xu et al., 2013; Cao et al., 2017). Based on eight-month-long *in situ* observations on the continental slope near Dongsha Island, Lee et al. (2012) found that incoherent internal tidal motion could explain three quarters of the total observed tidal energy. Furthermore, in the same area, Xu et al. (2013) found that semidiurnal internal tides were more incoherent than diurnal tides. Based on analysis of two nine-month-long moored current observation campaigns, Cao et al. (2017) investigated the coherent and incoherent internal tides in the NSCS, and they found that the coherent and incoherent features had spatial variations. As the seasonal variations of the background conditions and stratification are very weak in the near-bottom layer, our results show little seasonal variation in the proportions of the coherent and incoherent components.

As shown in Fig 3f, strong signals with periods of 16–32 d are obvious in the wavelet spectrum, corresponding to the passing of an anticyclonic mesoscale eddy (Figs 12a–c). We used a low-pass filter with a cutoff frequency of 0.05 cpd (period: 20 d) to obtain the currents induced by this eddy. As shown in Fig. 12e, the low-frequency currents in the near-bottom layer at the mooring sites were very weak. Before the passing of the eddy, the maximum and mean amplitude of the near-bottom velocity was less than 4.0 and 2.0 cm/s, respectively. However, the velocity was evidently enhanced during the passage of the eddy, with the maximum velocity reaching 11.9 cm/s. The mean amplitude of the velocity increased to 6.8 cm/s during the eddy period, i.e., more than three times greater than without the mesoscale eddy. Previous studies have also documented the effects of mesoscale eddies on the deep ocean. For example, Zhang et al. (2013) revealed enhanced near-bottom flows associated with the passing of a mesoscale eddy pair in the NSCS. Zhang et al. (2014) showed that surface-generated mesoscale eddies can have considerable influence on the deep-water dynamic sedimentary process in the NSCS.

6 Summary

The characteristics and seasonal variability of near-bottom currents on the continental slope in the NSCS were investigated based on two *in situ* observational campaigns conducted to the southeast of Dongsha Island. The original time series and wave-

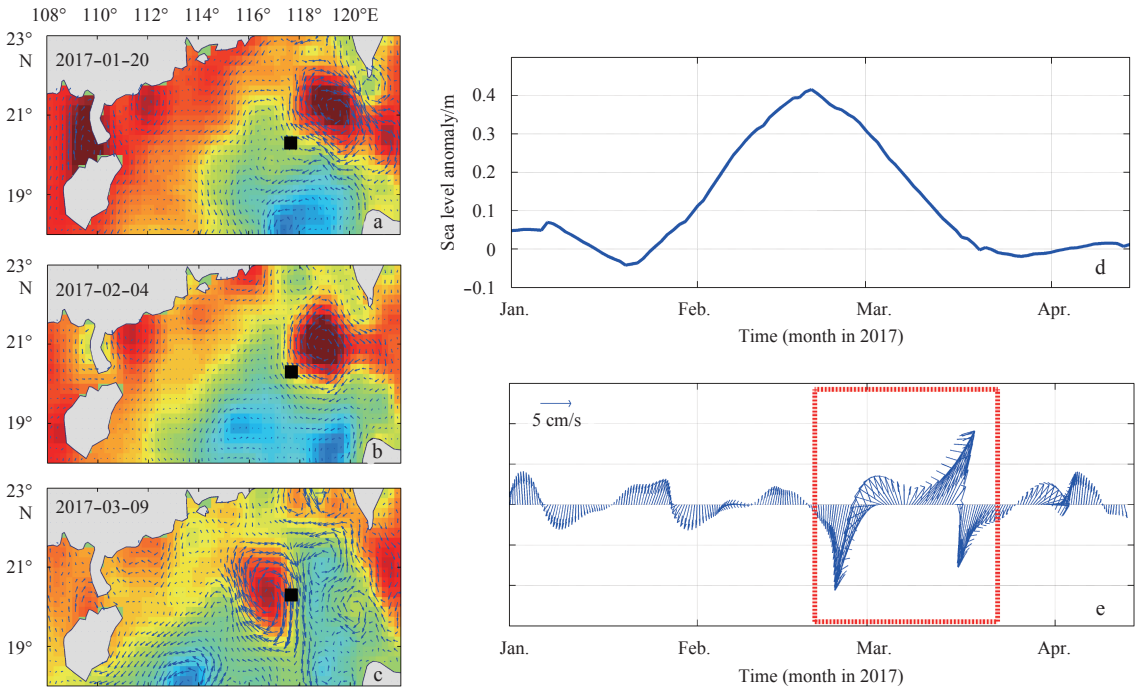

Fig. 12. Sea surface anomalies and currents at different times based on data from the AVISO website (https://www.aviso.altimetry.fr/) (a–c), sea surface anomaly time series of the observation site (d) and corresponding low-pass filtered currents recorded by the CM (e). Upward direction of the arrow represents northward.

let spectrum analysis demonstrated that the near-bottom currents are dominated by tidal currents, the variance of which could account for ~70% of the total current variance. The rotary spectra illustrated that the diurnal tidal currents are polarized with CW components that are ~10 times larger than the CCW components, whereas no obvious polarization characteristics were found for the semidiurnal currents. The wavelet shear spectra showed that diurnal tidal currents could induce strong vertical shear that could contribute to deep-ocean mixing. We conducted detailed analysis on the characteristics of the tidal currents. It was found that the diurnal tidal currents are stronger than the semidiurnal currents, irrespective of whether barotropic or baroclinic components. The diurnal tidal components in 2014 showed obvious seasonal variation with large amplitude in winter and summer and weak amplitude in spring and autumn. The study highlighted the importance of incoherent internal tidal constituents, which accounted for ~35% of the variance of the diurnal tidal currents and ~50% of the variance of the semidiurnal tidal currents. It was found that the proportions of the coherent and incoherent constituents did not change significantly in different seasons. In addition to the tidal currents, our results demonstrated that the deep-ocean current was enhanced markedly by the passage of an anticyclonic eddy. During the passing of the eddy, the mean magnitude of velocity was more than three times that without the mesoscale eddy, indicating the important role that mesoscale eddies might have in modulating the deep-ocean circulation of the NSCS.

Acknowledgements

We thank the crew who conducted the field measurements. We also thank the AVISO for the distribution of sea surface anomaly data (https://www.aviso.altimetry.fr/).

References

Alford M H, Peacock T, MacKinnon J A, et al. 2015. The formation and fate of internal waves in the South China Sea. Nature, 521(7550): 65–69

Beardsley R C, Duda T F, Lynch J F, et al. 2004. Barotropic tide in the Northeast South China Sea. IEEE Journal of Oceanic Engineering, 29(4): 1075–1086

Cao Anzhou, Guo Zheng, Lv Xianqing, et al. 2017. Coherent and incoherent features, seasonal behaviors and spatial variations of internal tides in the northern South China Sea. Journal of Marine Systems, 172: 75–83

Chen Hui, Xie Xinong, Zhang Wenyan, et al. 2016. Deep-water sedimentary systems and their relationship with bottom currents at the intersection of Xisha Trough and Northwest Sub-Basin, South China Sea. Marine Geology, 378: 101–113

Duda T F, Lynch J F, Irish J D, et al. 2004. Internal tide and nonlinear internal wave behavior at the continental slope in the northern south China Sea. IEEE Journal of Oceanic Engineering, 29(4): 1105–1130

Egbert G D, Erofeeva S Y. 2002. Efficient inverse modeling of Barotropic ocean tides. Journal of Atmospheric and Oceanic Technology, 19(2): 183–204

Garrett C, Kunze E. 2007. Internal tide generation in the deep ocean. Annual Review of Fluid Mechanics, 39(1): 57–87

Gonella J. 1972. A rotary-component method for analysing meteorological and oceanographic vector time series. Deep Sea Research and Oceanographic Abstracts, 19(12): 833–846

Guo Pu, Fang Wendong, Liu Changjian, et al. 2012. Seasonal characteristics of internal tides on the continental shelf in the northern South China Sea. Journal of Geophysical Research: Oceans, 117(C4): C04023

Hu Jianyu, Kawamura H, Hong H, et al. 2000. A review on the currents in the South China Sea: seasonal circulation, South China Sea warm current and Kuroshio Intrusion. Journal of Oceanography, 56(6): 607–624

Klymak J M, Alford M H, Pinkel R, et al. 2011. The breaking and scattering of the internal tide on a continental slope. Journal of Physical Oceanography, 41(5): 926–945

Lan Jian, Wang Yu, Cui Fengjuan, et al. 2015. Seasonal variation in the South China Sea deep circulation. Journal of Geophysical Research: Oceans, 120(3): 1682–1690

Lan Jian, Zhang Ningning, Wang Yu. 2013. On the dynamics of the South China Sea deep circulation. Journal of Geophysical Research: Oceans, 118(3): 1206–1210

Lee I H, Wang Yuhuai, Yang Y, et al. 2012. Temporal variability of internal tides in the northeast South China Sea. Journal of Geophysical Research: Oceans, 117(C2): C02013

Lei Shao, Li Xuejie, Geng Jianhua, et al. 2007. Deep water bottom current deposition in the northern South China Sea. Science in China Series D: Earth Sciences, 50(7): 1060–1066

Li Li, Qu Tangdong. 2006. Thermohaline circulation in the deep South China Sea basin inferred from oxygen distributions. Journal of Geophysical Research: Oceans, 111(C5): C05017

Lien R C, Tang T Y, Chang M H, et al. 2005. Energy of nonlinear internal waves in the South China Sea. Geophysical Research Letters, 32(5): L05615

Ma B B, Lien R C, Ko D S. 2013. The variability of internal tides in the Northern South China Sea. Journal of Oceanography, 69(5): 619–630

Pawlowicz R, Beardsley B, Lentz S. 2002. Classical tidal harmonic analysis including error estimates in MATLAB using T_TIDE. Computers & Geosciences, 28(8): 929–937

Shu Yeqiang, Wang Qiang, Zu Tingting. 2018. Progress on shelf and slope circulation in the northern South China Sea. Science China Earth Sciences, 61(5): 560–571

Su Jilan. 2004. Overview of the South China Sea circulation and its influence on the coastal physical oceanography outside the Pearl River Estuary. Continental Shelf Research, 24(16): 1745–1760

Torrence C, Compo G P. 1998. A practical guide to wavelet analysis. Bulletin of the American Meteorological Society, 79(1): 61–78

Wang Guihua, Xie Shangping, Qu Tangdong, et al. 2011. Deep South China Sea circulation. Geophysical Research Letters, 38(5): L05601

Xu Zhenhua, Yin Baoshu, Hou Yijun, et al. 2013. Variability of internal tides and near-inertial waves on the continental slope of the northwestern South China Sea. Journal of Geophysical Research: Oceans, 118(1): 197–211

Zhang Yanwei, Liu Zhifei, Zhao Yulong, et al. 2014. Mesoscale eddies transport deep-sea sediments. Scientific Reports, 4: 5937

Zhang Zhiwei, Zhao Wei, Tian Jiwei, et al. 2013. A mesoscale eddy pair southwest of Taiwan and its influence on deep circulation. Journal of Geophysical Research: Oceans, 118(12): 6479–6494

Zhao Zhongxiang, Klemas V, Zheng Quanan, et al. 2004. Remote sensing evidence for baroclinic tide origin of internal solitary waves in the northeastern South China Sea. Geophysical Research Letters, 31(6): L06302

Zheng Quanan, Susanto R D, Ho C R, et al. 2007. Statistical and dynamical analyses of generation mechanisms of solitary internal waves in the northern South China Sea. Journal of Geophysical Research: Oceans, 112(C3): C03021

Zheng Hongbo, Yan Pin. 2012. Deep-water bottom current research in the Northern South China Sea. Marine Georesources & Geotechnology, 30(2): 122–129